Chapter 11
The Shape of Spatial Spread

Abstract In previous chapters, we studied the speed of spread and the existence of traveling waves. In this chapter, we focus on the shape of traveling-wave profiles and more general patterns of spatial spread. We first provide an approximation scheme, based on asymptotic expansion, for the shape of a monotone wave. Then we explore the existence of nonmonotone waves as well as more complicated patterns of spread when the growth function has a stable two-cycle. We generalize the notion of the asymptotic spreading speed and discuss dynamic stabilization.

11.1 Monotone Versus Nonmonotone Scenarios

In the study of biological invasions, the speed of spatial spread of the invading organism is arguably the most important quantity. The theory in Chaps. 5 and 6 guarantees the existence of such a speed and, in some cases, also provides a simple formula for it, but leaves open many questions about the shape of an invasion front. When the growth function is monotone, the results in Chap. 5 also establish the existence of monotone traveling waves. Information about the steepness of the wave, say, would tell us how fast the invading population grows at any fixed location. When the growth function is not monotone, we would like to know more about the shape of the profile behind the initial invasion front; see Fig. 5.6. Will the profile converge to the positive steady state, and if so how fast? But many more scenarios could arise. Since the positive steady state of the nonspatial Ricker model may be unstable, there is no reason to believe that a traveling profile in the spatial model with Ricker dynamics—if it exists—would settle at that positive state. If it does not, then what are the dynamics of the population in the wake of the invasion front? Would a profile oscillate in ways comparable to those that we have seen in Sect. 4.4? In this chapter, we present various approaches to answer some of these questions.

The first part of this chapter is based on the analysis of traveling waves. We assume that there is a traveling-wave solution of speed c, i.e., a profile N that satisfies

F. Lutscher, *Integrodifference Equations in Spatial Ecology*, Interdisciplinary Applied Mathematics 49, https://doi.org/10.1007/978-3-030-29294-2_11

$$N(x+c) = Q[N](x) = \int_{-\infty}^{\infty} K(x-y)F(N(y))\mathrm{d}y\,. \tag{11.1}$$

In this notation, the profile travels to the left when $c > 0$, so that we impose the boundary conditions $N(-\infty) = 0$ and $N(\infty) = 1$. The profile travels to the right when $c < 0$ and the boundary conditions are interchanged. When the dispersal kernel is the Laplace or the exponential kernel, we can reduce this equation to a second- or first-order delay equation, which we can study via linearization and asymptotic expansion. This material was originally developed by Kot (1992).

In the second part, we consider the case where the positive steady state of the nonspatial growth function is unstable and there is a stable two-cycle. We study this case by considering the second-iterate operator $N_{t+2} = Q \circ Q[N_t]$. Some aspects of the traveling-wave analysis from the first part of this chapter can be extended to this case. More important, the theory from Chap. 5 can be adapted to yield the existence of *generalized spreading speeds* and various forms of traveling profiles that appear after the initial invasion front and travel more slowly. This material originates in the thesis of Bourgeois (2016). The existence of two or more distinct traveling profiles at different speeds leads to *stacked waves* and the phenomenon of dynamic stabilization.

11.2 Asymptotic Expansion of Monotone Traveling Waves

When the growth function is of Beverton–Holt type (monotone, concave down) and the dispersal kernel is exponentially bounded, then there exist monotone traveling-wave solutions (11.1) of the IDE for every $c \geq c^*$; see Chap. 5, Theorem 5.2. We obtain a unique (leftward-moving) solution if we fix the density at one point, e.g., $N(0) = 1/2$.

When the dispersal kernel is the Laplace kernel (2.27), we can use repeated differentiation as in (3.7) to turn equation (11.1) into the second-order delay differential equation

$$N''(x+c) = a^2[N(x+c) - F(N(x))]\,. \tag{11.2}$$

A constant solution of this equation satisfies $N = F(N)$; i.e., it is a fixed point of the nonspatial dynamics. By our assumptions on F, there are exactly two such fixed points, namely $N = 0$ and $N = 1$, the asymptotic values of the traveling wave. We are looking for a solution that connects these two points.

To apply asymptotic expansion, we need to identify a small parameter in the equation. We rescale space by setting $x = zc$ and define $\tilde{N}(x/c) = N(x)$. Using the chain rule and dropping the tilde, we find the equation

$$\frac{1}{(ac)^2}N''(z+1) + F(N(z)) - N(z+1) = 0\,. \tag{11.3}$$

We now consider $\epsilon = 1/(ac)^2$ as our small parameter. We know that the smallest traveling-wave speed $\hat{c} = c^*$ is an increasing function of the growth rate at low density $F'(0)$ for fixed $a > 0$. Hence, we can make ϵ small by making $F'(0)$ large.

We expand the solution $N(z)$ of (11.3) in a perturbation series

$$N(z) = N^{(0)}(z) + \epsilon N^{(1)}(z) + \epsilon^2 N^{(2)}(z) + \dots \,. \tag{11.4}$$

Inserting this expansion into (11.3), we obtain an infinite system of equations. The two lowest-order equations are

$$N^{(0)}(z+1) = F(N^{(0)}(z))\,, \tag{11.5}$$

$$N^{(1)}(z+1) = F'(N^{(0)}(z))N^{(1)}(z) + [N^{(0)}]''(z+1)\,. \tag{11.6}$$

The lowest-order equation looks like the simple nonspatial equation. The difference is that the equation here is meant to hold for a continuous variable $z \in \mathbb{R}$ and not just for a discrete set $z \in \mathbb{N}$. Fortunately, we have an explicit solution of (11.5) if F is the scaled Beverton–Holt function (2.13), namely

$$N^{(0)}(z) = \frac{R^z}{1+R^z}\,; \tag{11.7}$$

see (2.16). This solution satisfies the two boundary conditions, $N^{(0)}(-\infty) = 0$ and $N^{(0)}(\infty) = 1$, and the condition at zero, $N^{(0)}(0) = 1/2$. It also defines a continuous function on $\mathbb{R}$. Hence, we have found an approximation to lowest order.

Comparing this lowest-order approximation to numerical simulations of the traveling front, we see that the approximation is very good even when ϵ is on the order of unity. The left plot in Fig. 11.1 shows that the two curves are virtually

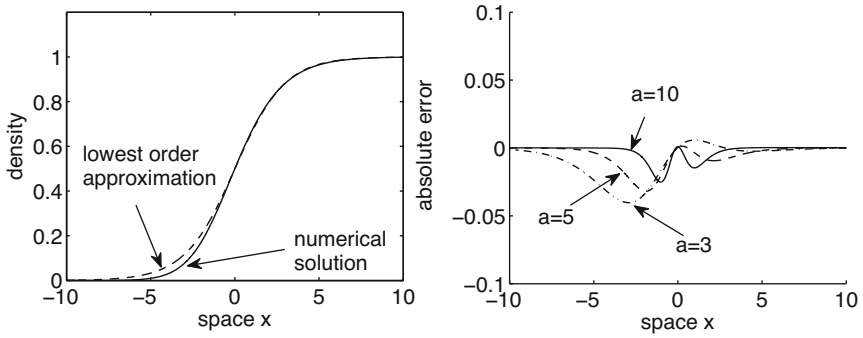

Fig. 11.1 Comparison of the numerically obtained shape of a traveling front and its lowest-order approximation. **Left:** The two densities. **Right:** The absolute error, $N(x) - N^{(0)}(x)$. The growth function is the Beverton–Holt function with $R = 1.25$. The dispersal kernel is the Laplace kernel with $a = 5$ (left plot) and values of a as indicated (right plot).

indistinguishable and that the absolute error, defined as $N(x) - N^{(0)}(x)$ (right plot), is small for $\epsilon = 1.0139$. As discussed above, ϵ decreases as R increases, so that the approximation should become even better. As a decreases and dispersal distances increase, the error increases in size and in spatial extent.

Kot (1992) proceeds to solve the equation for $N^{(1)}$ in (11.6) explicitly, but the computations are lengthy and the gain is relatively small since the zero-order approximation is already good. Instead, we consider a different example where the calculations of the higher-order term are somewhat simpler and provide greater improvement.

Asymptotics for the Exponential Kernel

The exponential kernel

$$K(x) = \begin{cases} a\,\exp(ax)\,, & x \le 0\,, \\ 0\,, & x > 0\,, \end{cases} \tag{11.8}$$

is the (scaled) "left half" of the Laplace kernel and allows leftward spread only. The moment-generating function is

$$M(s) = \frac{a}{a-s}\,. \tag{11.9}$$

The parametric representation of c according to (5.22) can be written as (compare (5.26))

$$ac = 1 + \bar{s}\,, \qquad R = \frac{\mathrm{e}^{\bar{s}}}{1+\bar{s}}\,, \tag{11.10}$$

with $\bar{s} = -\frac{s}{a-s}$. The defining equation for the traveling front with the exponential kernel turns into

$$N(x+c) = a\int_x^\infty \mathrm{e}^{a(x-y)} F(N(y))\mathrm{d}y\,. \tag{11.11}$$

Differentiating once, we obtain the first-order delay differential equation

$$N'(x+c) + a[F(N(x)) - N(x+c)] = 0\,. \tag{11.12}$$

Similar to the procedure for the Laplace kernel, we scale space by setting $x = zc$, introduce the small parameter $\epsilon = 1/(ac)$, and expand $N(z)$ in a perturbation series. The two lowest-order equations are

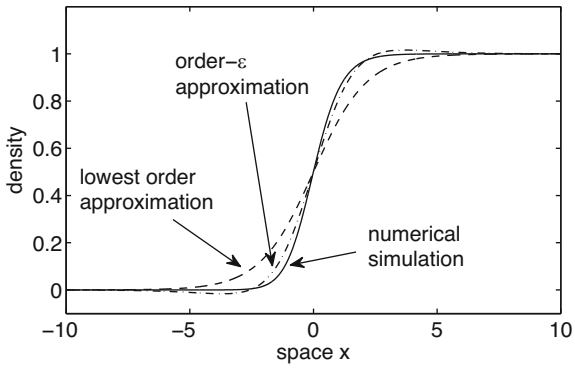

Fig. 11.2 Comparison of the numerically obtained shape of a traveling front and its two lowest-order approximations. The growth function is the Beverton–Holt function with $R = 1.5$. The dispersal kernel is the exponential kernel with $a = 5$.

$$N^{(0)}(z+1) = F(N^{(0)}(z))\,, \tag{11.13}$$

$$N^{(1)}(z+1) = F'(N^{(0)}(z))N^{(1)}(z) + [N^{(0)}]'(z+1)\,. \tag{11.14}$$

The equation for $N^{(0)}$ is the same as (11.5), so that we already have its solution in (11.7). The plot in Fig. 11.2 shows that this approximation is not as close as for the Laplace kernel in the previous section. To improve the approximation, we calculate the term of order ϵ.

Substituting the expressions for $N^{(0)}$ and $F'(N)$ into (11.14), we arrive at

$$N^{(1)}(z+1) = \frac{R(1+R^z)^2}{(1+R^{z+1})^2}N^{(1)}(z) + \ln(R)\frac{R^{z+1}}{(1+R^{z+1})^2} \tag{11.15}$$

or, after rearranging,

$$\frac{(1+R^{z+1})^2}{R^{z+1}}N^{(1)}(z+1) = \frac{(1+R^z)^2}{R^z}N^{(1)}(z) + \ln(R)\,. \tag{11.16}$$

Hence, the expression $U(z) = \frac{(1+R^z)^2}{R^z}N^{(1)}(z)$ satisfies the simple recursion relation

$$U(z+1) = U(z) + \ln(R)\,. \tag{11.17}$$

To find its solution, we need an initial condition. Since $N^{(0)}(0) = N(0) = 1/2$, the requirement is $N^{(1)}(0) = 0 = U(0)$. Therefore, the solution for U is $U(z) = z\ln(R)$. As before, this solution is initially only determined for $z \in \mathbb{N}$, but we notice that it is a continuous function for all $z \in \mathbb{R}$.

The resulting approximation for $N(x)$ in the original parameters is

$$N(x) = \frac{R^{x/c}}{1+R^{x/c}} + \frac{1}{ac}\frac{x}{c}\frac{\ln(R)R^{x/c}}{(1+R^{x/c})^2} + O(\epsilon^2)\,. \tag{11.18}$$

The improvement of this approximation over the previous one is obvious in Fig. 11.2.

The approximation procedure presented here requires that we find an explicit solution of the zero-order equation analytically. Numerical methods would only allow us to calculate approximations defined on the integers. In particular, we cannot easily use the method to study the shape of solutions when the growth function is not monotone. In the following section, we take a linearization-based approach to distinguish between monotone and nonmonotone solutions.

11.3 Traveling Waves in the Phase Plane

We return to Eq. (11.2), but now we treat it as a dynamical system in the phase plane. We turn the second-order equation into a pair of first-order equations and let $y = x + c$ to obtain

$$N'(y) = n(y)\,, \qquad n'(y) = a^2[N(y) - F(N(y-c))]\,. \tag{11.19}$$

We point out that since the equation has a delay, the phase space is really infinite dimensional and the representation in the "phase plane" is somewhat misleading. For example, solutions of this system can cross in the phase plane. Nonetheless, the visualization in two dimensions turns out to be helpful.

The steady states of system (11.19) are of the form $(N^*, 0)$, where N^* is a solution of $F(N) = N$. A traveling wave of the IDE is a heteroclinic connection between the steady states $(0, 0)$ and $(1, 0)$. A necessary condition for such a connection to exist is that $(0, 0)$ be unstable and $(1, 0)$ have at least one stable direction. A monotone front requires that the eigenvalue at $(1, 0)$ be real and negative, whereas a front with damped spatial oscillations at $(1, 0)$ requires it to have nonzero imaginary and negative real part.

Figure 11.3 shows a monotone and a nonmonotone front for the IDE with Ricker dynamics together with their phase-plane representations. In the nonspatial Ricker model from (2.19), we have $F'(1) = 1 - r$. Solutions approach one in a monotone way when $0 < r \leq 1$ and in an oscillatory way when $1 < r < 2$. When $r > 2$, stability is lost, and cyclic or chaotic behavior appears. Accordingly, the lowest-order approximation to the traveling wave from (11.5) predicts monotone traveling fronts when $0 < r \leq 1$ and nonmonotone fronts for some $1 < r < 2$. Dispersal appears to have a dampening effect since Fig. 11.3 shows a monotone wave for some $r > 1$.

To study the stability of the two steady states in the phase plane, we linearize the traveling-wave equation. It is easier to work with (11.3). The scaling does not affect the sign of the eigenvalue. We find the transcendental eigenvalue problem

$$1 - \frac{\lambda^2}{a^2 c^2} = F'(N^*)\mathrm{e}^{-\lambda}\,. \tag{11.20}$$

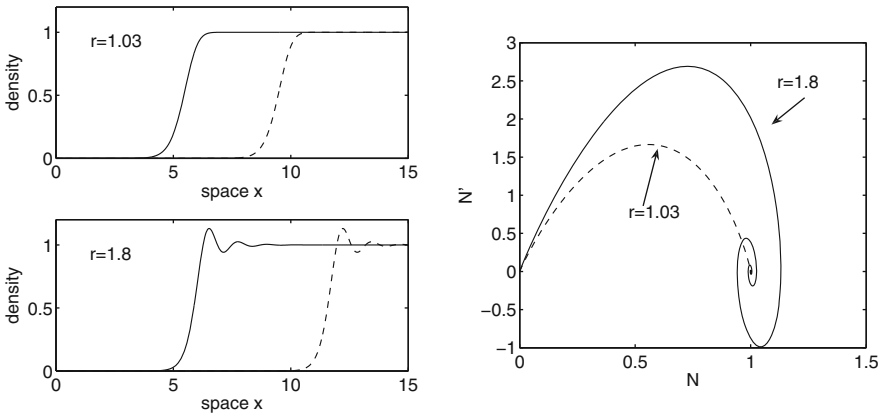

Fig. 11.3 **Left:** Traveling fronts with Ricker dynamics and a Laplace kernel can show a monotone profile ($r = 1.03$, top) or damped spatial oscillations ($r = 1.8$, bottom). The two profiles (solid and dashed lines) are taken 10 generations apart. **Right:** Phase-plane representations of the invasion fronts. The dispersal parameter is $a = 6$.

Alternatively, we linearize (11.19) and scale the eigenvalue; see Chap. 4 in Bourgeois (2016). We ask for conditions such that the parabola on the left intersects the exponential on the right. We distinguish three cases.

Case 1: $F'(N^*) > 1$

If $F'(N^*) > 1$, the parabola on the left-hand side of (11.20) and the exponential on the right cannot intersect for $\lambda < 0$. There are two positive intersections when c is large enough but none when c is small. We illustrate this case in Fig. 11.4, top left panel. The thick solid curve represents the right-hand side of (11.20); the thin solid (dashed) curve represents the left-hand side for small (large) c. The critical case, in which the curves are tangent, is given by the pair of equations

$$1 - \frac{\lambda^2}{a^2c^2} = F'(N^*)\mathrm{e}^{-\lambda} \quad \text{and} \quad \frac{2\lambda}{a^2c^2} = F'(N^*)\mathrm{e}^{-\lambda}\,. \tag{11.21}$$

These two equations lead precisely to the defining equations for the minimal speed of a traveling front with λ in place of $\tilde{s}$; see (5.26). This situation may arise at the zero state where $F'(0) = R_0 > 1$. Hence, the zero state in the phase plane is unstable precisely when the speed is at least the minimal speed. We have recovered the result from Theorem 5.1 that there can be no biologically meaningful traveling waves for $c < \hat{c}$.

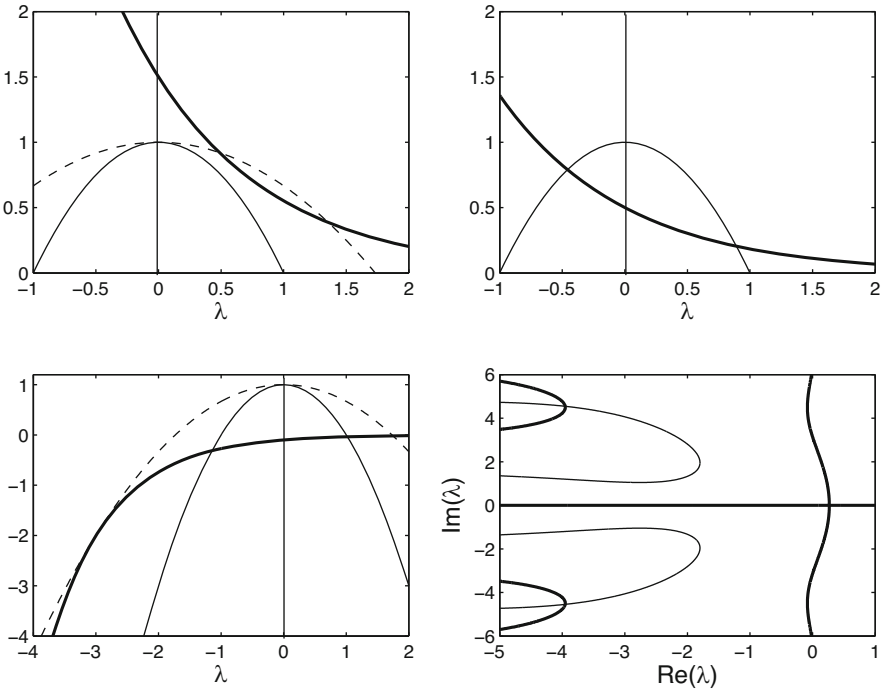

Fig. 11.4 Illustrating the potential roots of the eigenvalue problem in (11.20) as intersections of curves. **Top left:** When $F'(0) > 1$, there is a critical value for c for which a positive eigenvalue exists. **Top right:** When $0 < F'(1) < 1$, there is always one positive and one negative real eigenvalue. **Bottom left:** When $F'(1) < 0$, there is one positive eigenvalue, and there can be up to two negative eigenvalues. **Bottom right:** When $F'(1) < 0$ and there are no negative eigenvalues, there can be complex eigenvalues with negative real part. The thick (thin) curves indicate where the first (second) condition in (11.22) is satisfied. The intersection points indicate the eigenvalues. They all have negative real parts.

Case 2: $0 \le F'(N^*) < 1$

If $0 \le F'(N^*) < 1$, there is exactly one positive and one negative solution of (11.20); see Fig. 11.4, top right panel. As before, the thick (thin) curve represents the right-hand (left-hand) side. This situation arises at the positive steady state with the Beverton–Holt function but also with the Ricker function when $0 < r < 1$. The necessary conditions for the existence of a monotone traveling wave are satisfied.

Case 3: $F'(N^*) < 0$

When the slope of the updating function at the positive steady state is negative, (11.20) always has one positive solution. When c and/or $|F'(N^*)|$ are small, there

are two negative solutions; when they are large, there is no negative solution; see Fig. 11.4, bottom left panel. As usual, the thick curve represents the exponential in (11.20); the thin solid (dashed) curve represents the quadratic with small (large) c. There are two negative intersections for small c. The dashed curve shows the critical case where the curves are tangent, which leads to the pair of equations (11.21).

When there are no real negative solutions, we consider complex-valued solutions. We write $\lambda = \alpha + \mathrm{i}\beta$ and split the equation in (11.20) into real and imaginary parts, namely

$$1 - \frac{\alpha^2 - \beta^2}{a^2 c^2} = F'(N^*)\mathrm{e}^{-\alpha}\cos(\beta)\,, \qquad \frac{2\alpha\beta}{a^2 c^2} = -F'(N^*)\mathrm{e}^{-\alpha}\sin(\beta)\,. \tag{11.22}$$

The bottom right panel in Fig. 11.4 illustrates the solution curves of these equations in the complex plane. Their intersection points correspond to eigenvalues.

We return to the case of the Ricker function in Fig. 11.3. When $r = 1.03$, we have $F'(1) = -0.03 < 0$. As $|F'(N^*)|$ is small, we have two negative eigenvalues as in the bottom left panel of Fig. 11.4. Hence, there can be a monotone traveling wave, as observed in Fig. 11.3. When $r = 1.8$, we have $F'(1) = -0.8 < 0$. As $|F'(N^*)|$ is now much larger, we have no negative eigenvalues but complex eigenvalues with negative real parts, as in the bottom right panel of Fig. 11.4. Hence, there cannot be a monotone traveling wave, but there is a wave with decaying oscillations around one, as observed in Fig. 11.3. For the existence of traveling waves, see Sect. 5.4.

11.4 Invasion Dynamics with a Two-Cycle

So far, we have assumed that the positive state $N^* = 1$ is stable for the growth dynamics. Without this assumption, there is no reason to believe that a traveling wave could exist, since the dynamic behavior in the wake of a wave is often determined by the stable steady states for the nonspatial equation. What can we expect if there is no stable steady state? Kot (1992) finds a "traveling two-cycle" in numerical simulations; see also Kot (2003). We illustrate this kind of solution to motivate the subsequent analysis.

The Ricker map, $F(N) = N\exp(r(1 - N)$, has a globally stable two-cycle for $r = 2.2$, with densities $0 < n_- < 1 < n_+$, satisfying $F(F(n_-)) = F(n_+) = n_-$. The invasion dynamics of the spatial model are shown in the left plot in Fig. 11.5. At the invasion front, the density increases from zero, overshoots the state $N = 1$, and then shows damped spatial oscillations to that state in the wake. Somewhere behind the invasion front, a second front alternates between increasing to n_+ in even generations (dashed) and decreasing to n_- in odd generations (solid). The right plot in Fig. 11.5 reveals that the first front with the damped oscillations travels faster than the alternating second front that connects to n_- and n_+, respectively. Hence, the term "traveling two-cycles" (Kot 1992) could be misleading because this is not a

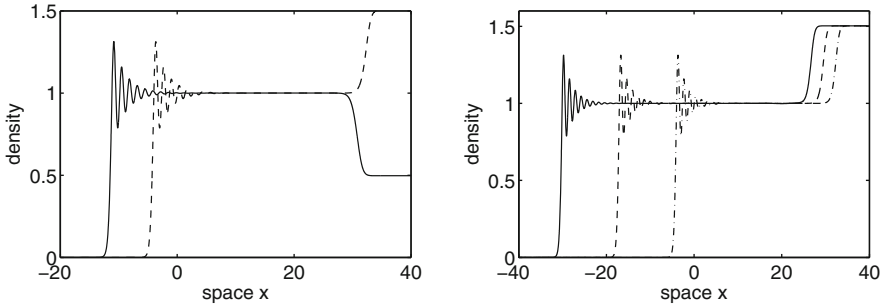

Fig. 11.5 Invasion dynamics with a stable two-cycle. **Left:** The profile of the front at odd generations (solid) connects with the lower value of the nonspatial two-cycle, n_-, whereas the profile at even generations (dashed) connects with the higher values, n_+. The two profiles are 11 generations apart. **Right:** Plotting the profile 20 generations apart shows that the nonmonotone first front travels faster than the monotone second front. Parameters are $r = 2.2$ for the Ricker growth function and $a = 6$ for the Laplace kernel. The initial condition is a step function.

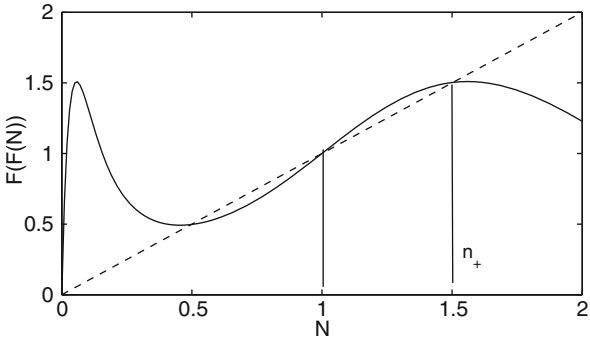

Fig. 11.6 Plot of the second-iterate map of the Ricker function with $r = 2.2$.

single profile traveling at a constant speed but rather two different objects traveling at different speeds.

Few authors have considered this problem. Theorem 5.3 guarantees the existence of a spreading speed even when the positive state is unstable. Hsu and Zhao (2008), Li et al. (2009), and Yu and Yuan (2012) prove the existence of a traveling-wave profile under some conditions, but the shape of the profile behind the initial front is unclear. Bourgeois (2016) provides a more detailed study of the spatial invasion dynamics with an unstable fixed point; see also Bourgeois et al. (2018) and Bourgeois et al. (2019). We present some of these results here.

To gain some preliminary insight into the second front, we consider the iteration of two generations. For the nonspatial Ricker model with $r = 2.2$, the map $N_{t+2} = F(F(N_t))$ has four fixed points. The fixed points of F and each of the points of the two-cycle of F are fixed points of $F \circ F$; see Fig. 11.6. The points zero and one are unstable, whereas $n_\pm$ are stable. The corresponding two-generation IDE is

$$N_{t+2}(x) = Q \circ Q[N_t](x) = \int K(x-y) F\left(\int K(y-z) F(N_t(z)) \mathrm{d}z\right) \mathrm{d}y\,. \tag{11.23}$$

We are looking for a monotone front that connects $N = 1$ with $N = n_+$ or $N = n_-$. Such a front satisfies the equation

$$N(x + 2c) = \int_{-\infty}^{\infty} K(x - y) F\left(\int_{-\infty}^{\infty} K(y - z) F(N(z)) \mathrm{d}z\right) \mathrm{d}y \,. \tag{11.24}$$

We write the speed as $2c$ because we consider two generations in the equation. We study its behavior near $N = 1$ by linearization. The linearized equation is

$$n(x + 2c) = F'(1)^2 \int \int K(x - y) K(y - z) n(z) \mathrm{d}y \, \mathrm{d}z \,. \tag{11.25}$$

Taking an exponential transform or substituting an exponential profile leads to the dispersion relation

$$\mathrm{e}^{2sc} = (F'(1))^2 M^2(s) \,, \tag{11.26}$$

where $M(s)$ is the moment-generating function of K as usual. After taking square roots, we find the minimal speed at which a profile in the linearized equation can travel as

$$\hat{c}_1 = \frac{1}{s} \ln(|F'(1)| M(s)) \,. \tag{11.27}$$

For the Ricker function, we have $F'(0) = \mathrm{e}^r$ and $F'(1) = 1 - r$, so that $F'(0) > |F'(1)|$ for all $r > 0$. In particular, the slowest speed for a front in the linearized equation at zero is always larger than for the linearized equation at one. For the parameters in Fig. 11.5, the speed of the initial front is $c_0 = 0.67$, whereas the speed of the second front is $c_1 = 0.14$. The plateau region at level $N = 1$ between the first and second fronts grows by the difference $c_0 - c_1$ per generation. In particular, even though the state $N = 1$ is unstable for the nonspatial dynamics, it appears stable for a potentially long time in the spatial model. This same phenomenon, but in a two-component reaction–diffusion model, has been termed dynamic stabilization by Malchow et al. (2008).

11.5 Generalized Spreading Speeds

To study the speed of spread of the second front that we observe in the simulations in Fig. 11.5, we generalize the definition of the asymptotic spreading speed in (5.31) to allow for the state ahead of the front to be positive (Bourgeois 2016; Bourgeois et al. 2018). The construction is a slight extension of the one by Weinberger (1982).

We consider an operator $\widetilde{Q}$ that acts on continuous functions on $\mathbb{R}$. We assume that there are two constants $0 \leq \pi_0 < \pi_1 < \infty$ such that $\widetilde{Q}[\pi_i] = \pi_i$ for the

corresponding constant functions. We denote the set of all continuous functions with values in $[\pi_0, \pi_1]$ as $\mathscr{C}_{[\pi_0,\pi_1]}$ and define a sequence of functions by the iteration $N_{t+1} = \widetilde{Q}[N_t]$.

Definition 11.1 The value $c^*_{(\pi_0,\pi_1)}$ is called the *generalized asymptotic spreading speed* of $\widetilde{Q}$ from π_0 to π_1 if the following conditions hold:

(i) For any $N_0 \in C_{[\pi_0,\pi_1]}$ such that $N_0 - \pi_0$ has compact support,

$$\lim_{t\to\infty} \sup_{|x|\geq ct} N_t(x) = \pi_0 \text{ for all } c > c^*_{(\pi_0,\pi_1)} . \tag{11.28}$$

(ii) For any $N_0 \in C_{[\pi_0,\pi_1]}$ such that $N_0 - \pi_0 \not\equiv 0$,

$$\lim_{t\to\infty} \inf_{|x|\leq ct} N_t(x) = \pi_1 \text{ for all } c \in (0, c^*_{(\pi_0,\pi_1)}) . \tag{11.29}$$

For $\pi_0 = 0$ and $\pi_1 = 1$, this definition agrees with Definition 5.1; i.e., $c^*_{(0,1)} = c^*$. If $\pi_0 = 0$, we can always achieve $\pi_1 = 1$ by rescaling.

The existence of a generalized spreading speed and associated traveling waves for operator $\widetilde{Q}$, satisfying appropriate conditions, follows from Theorem 5.1.

Theorem 11.1 *Assume that operator $\widetilde{Q}$ acts on the space of continuous functions $C_{[\pi_0,\pi_1]}$ as follows:*

(i) Translation invariance: $\widetilde{Q}[N(\cdot - a)](x) = \widetilde{Q}[N](x - a)$.
(ii) Invariance on $C_{[\pi_0,\pi_1]}$: $N \in C_{[\pi_0,\pi_1]} \Rightarrow \widetilde{Q}[N] \in C_{[\pi_0,\pi_1]}$.
(iii) Fixed points: $\widetilde{Q}[\pi_0] = \pi_0$, $\widetilde{Q}[\pi_1] = \pi_1$, $\widetilde{Q}[\alpha] > \alpha$ for $\alpha \in (\pi_0, \pi_1)$.
(iv) Monotonicity: $\pi_0 \leq N \leq \tilde{N} \leq \pi_1 \Rightarrow \widetilde{Q}[N] \leq \widetilde{Q}[\tilde{N}]$.
(v) Continuity: If $\{f_t\} \subset C_{[\pi_0,\pi_1]}$ and $f_t \to f$ uniformly on compact subsets of $\mathbb{R}$, then $\widetilde{Q}[f_t] \to \widetilde{Q}[f]$ pointwise as $t \to \infty$.
(vi) Compactness: Every sequence $\{f_j\}$ in $C_{[\pi_0,\pi_1]}$ has a subsequence $\{f_{j_i}\}$ such that $\{\widetilde{Q}[f_{j_i}]\}$ converges uniformly on every bounded subset of $\mathbb{R}$.

Then there exists a generalized spreading speed, $c^*_{(\pi_0,\pi_1)}$, for $\widetilde{Q}$ from π_0 to π_1. For all $c \geq c^*_{(\pi_0,\pi_1)}$, there exists a monotone traveling-wave solution $W(x - ct)$ with $W(-\infty) = \pi_1$ and $W(\infty) = \pi_0$.

Proof We construct an operator Q on $C_{[0,\pi_1-\pi_0]}$ as $Q[f] = \widetilde{Q}[f + \pi_0] - \pi_0$. This operator inherits all the qualitative properties from $\widetilde{Q}$, shifted to the interval $[0, \pi_1 - \pi_0]$. Hence, it satisfies the assumptions of Theorem 5.1, which guarantees the existence of a spreading speed and traveling waves. □

We want to apply this theorem to the second-iterate operator

$$\widetilde{Q}[N](x) = Q \circ Q[N](x) = \int K(x - y) F\left(\int K(y - z) F(N(z)) \mathrm{d}z\right) \mathrm{d}y . \tag{11.30}$$

The following theorem gives conditions on F for the existence of a generalized spreading speed and monotone traveling waves (Bourgeois 2016; Bourgeois et al. 2018).

Theorem 11.2 *Assume that K is continuous and that its moment-generating function is bounded for at least one nonzero value. Let F be a growth function that satisfies the following conditions:*

(i) *F is bounded and continuously differentiable.*
(ii) *F has exactly one stable two-cycle, i.e., there exist $n_\pm$ such that $0 < n_- < 1 < n_+$, $F(n_-) = n_+$ and $F(n_+) = n_-$, and all nonnegative initial conditions converge to this two-cycle under the map $N_{t+1} = F(N_t)$.*
(iii) *$N = 1$ is the only fixed point of F on the interval $[n_-, n_+]$.*
(iv) *$F'(1) < -1$.*
(v) *F is nonincreasing on the interval $[n_-, n_+]$.*

Then, there exists a spreading speed $c^*_{(1,n_+)}$ for the operator $\widetilde{Q}$ in (11.30) from one to n^+. Furthermore, for every $c \geq c^*_{(1,n_+)}$, there exists a monotone traveling-wave profile $W(x - ct)$ with $W(-\infty) = n_+$ and $W(\infty) = 0$.

Proof Translation invariance, continuity, and compactness of $\widetilde{Q}$ follow from the corresponding properties of Q. Function F maps the interval $[1, n_+]$ into $[n_-, 1]$, and vice versa. Hence, if $N \in [1, n_+]$, then $Q[N] \in [n_-, 1]$ and also $Q(Q[N]) \in [1, n_+]$. Therefore, $C_{[1,n_+]}$ is invariant under $\widetilde{Q}$. Since $F(1) = 1$ and $F(F(n_+)) = n_+$, we have $\widetilde{Q}(1) = 1$ and $\widetilde{Q}(n_+) = n_+$ in the sense of constant functions. From *(iv)* we have $(F \circ F)'(1) > 1$, and hence $F(F(\alpha)) > \alpha$ for some $\alpha > 1$. Since there is no fixed point between one and n_+, we must have $F(F(\alpha)) > \alpha$ for $\alpha \in (1, n_+)$. The same relation holds for constant functions under $\widetilde{Q}$. To show monotonicity, assume that $1 \leq N(x) \leq \tilde{N}(x) \leq n_+$. Then by *(v)*, we have $1 \geq F(N(x)) \geq F(\tilde{N}(x)) \geq n_-$ and hence also $1 \geq Q[N] \geq Q[\tilde{N}] \geq n_-$. But then we repeat the argument, since F maps $[n_-, 1]$ into $[1, n_+]$, and we obtain $1 \leq Q(Q[N]) \leq Q(Q[\tilde{N}]) \leq n_+$. □

The monotonicity assumption *(v)* is satisfied for the Ricker function with $2 < r < 2.2565$ and for the logistic function with $2 < r < 2.2362$, respectively. For larger values of r, function F is not monotone in the interval $[n_-, n_+]$. Under certain conditions, the existence of a generalized spreading speed for $\widetilde{Q}$ can still be shown. The key idea is to construct operators $\widetilde{Q}^\pm$ that bound $\widetilde{Q}$, just as we constructed operators $Q^\pm$ that bounded Q for overcompensatory dynamics in Sect. 5.4. Details can be found in the thesis by Bourgeois (2016) and in Bourgeois et al. (2018).

Theorem 11.2 and its generalizations to nonmonotone dynamics have an immediate analogue on the interval $[n_-, 1]$. By applying the one-step operator Q to any solution of the two-step operator $\widetilde{Q}$, we obtain traveling waves that connect one to n_-.

The theorem gives the existence of a spreading speed, but no simple formula to calculate it. In particular, it is not known whether the linear conjecture holds, i.e., whether the generalized spreading speed $c^*_{(1,n_+)}$ is determined by the linearization at 0. Based on numerical simulations, Bourgeois (2016) conjectures that the speed is linearly determined and that $c^*_{(1,n_+)} = \hat{c}_1$ from (11.27).

11.6 Further Reading

The dynamics of the nonspatial Ricker map range from monotone or nonmonotone convergence to a unique positive steady state to chaotic dynamics. We only discussed spreading phenomena in a few cases of a stable steady state or a stable two-cycle. The ideas presented here can be and have been applied to higher-order cycles. For example, Bourgeois (2016) uses the fourth power of operator Q to study spreading dynamics with four-cycles; see also the discussion in Bourgeois et al. (2018). Seemingly chaotic behavior in the wake of an invasion can be observed in numerical simulations; see Andersen (1991) and Li et al. (2009).

Bourgeois et al. (2018) do not address the stability of the traveling profiles in the case where the growth function has a stable two-cycle. They use step functions as initial conditions in their simulations. The resulting shapes (e.g., Fig. 11.5) appear to be stable in some sense since they were obtained by two independent numerical schemes. On the other hand, Li et al. (2009) prove the existence of traveling waves for operator Q and find a spatially oscillating profile by numerical fixed-point iteration (see Fig. 4 in their paper). It is unclear whether this profile is stable for the dynamics of the IDE.

Many more phenomena can occur with overcompensatory dynamics. For example, since $\widetilde{Q}$ has the three positive fixed points, $n_- < 1 < n_+$, and since n_- and n_+ are stable, there could be a bistable front connecting n_- to n_+. From Theorem 6.2, we know that a bistable front of operator Q can and does exist for only one speed c^*. The techniques in Lui (1983) unfortunately do not apply for proving uniqueness of the speed in this case. However, Bourgeois et al. (2018) show that if the speed is unique, then it has to be zero, i.e., the wave is a standing wave. Numerical simulations suggest the existence of a standing wave; see Fig. 9 in Bourgeois et al. (2018).

We can extend the phase-plane approach from Sect. 11.3 to study spreading phenomena and dynamic stabilization as the growth parameter in the Ricker function increases so that the nonspatial dynamics exhibit oscillations. There is evidence for a Hopf bifurcation as the intersection points of the thin and thick curves in the bottom right panel in Fig. 11.4 move across the imaginary line to have positive real parts; see Fig. 4.19 by Bourgeois (2016) for an illustration and Bourgeois et al. (2019) for more details.

The theory and examples in this chapter all assumed that the growth dynamics have no Allee effect. Schreiber (2003) studies several nonspatial models with Allee

effect and Ricker dynamics and finds that overcompensation and a strong Allee effect could lead to complex extinction dynamics. Sullivan et al. (2017) combine Allee dynamics and overcompensation with spatial spread and find pulsating traveling waves. Otto (2017) in his PhD thesis also studies an IDE that includes an Allee effect and overcompensation. He finds a novel type of solution that neither spreads nor retreats but stays in place with compact support in a homogeneous environment.